ELSEVIER

Photo-induced deformation behavior depending on the glass transition temperature on the surface of urethane copolymers containing a push–pull type azobenzene moiety

Osamu Watanabe *, Mamiko Narita, Taiji Ikawa, Masaaki Tsuchimori

Toyota Central Research and Development Labs, Nagakute, Aichi 480-1192, Japan

Abstract

Urethane copolymers containing a push–pull type azobenzene moiety with the same dye content were synthesized to investigate the relationship between photo-induced deformation and molecular mobility. The copolymers exhibit different glass transition temperatures (T_g), from 46 to 143 °C, due to their different main chain structures. An indented nanostructure induced by the optical near field around the polystyrene microspheres and a surface relief grating (SRG) induced by exposure to a two-beam interference pattern were examined using films of copolymers. We found the dependency of the deformation efficiency on T_g was inverted depending on the irradiation power. The deformation depth increased with T_g under high power irradiation in both the indented nanostructure and the SRG forming experiments. In contrast, the deformation depth of the SRG decreased with increasing T_g under low power irradiation. The discovery of this inverted tendency suggests that, in addition to the molecular mobility, we should consider other factors in the deformation mechanism, such as the recovery of deformation, the degree of plasticization, and the thermal effects.

© 2006 Elsevier Ltd. All rights reserved.

Keywords: Azopolymer; Photo-induced deformation; Glass transition temperature

1. Introduction

During the past few decades, polymeric systems containing azobenzene derivatives have been attracting considerable attention because of their potential use in various photonic applications [1–6]. Among these polymeric systems, azopolymers containing push–pull type azobenzene moieties that include an electron withdrawing group and an electron donating group show an interesting response to light, due to their unique photoisomerization properties. The trans-form of the azobenzene moiety can be photoisomerized to the cis-form by light irradiation, and cis–trans back-isomerization can occur thermally and/or photochemically during irradiation [7]. This cyclic isomerization process of the azobenzene moiety generates effective changes in the optical and physical properties of the polymer matrix [2,8,9]. When the azopolymer is irradiated with linearly polarized light, the amount of the azobenzene moiety that is oriented perpendicular to the

polarization direction increases with time due to the cyclic isomerization, and so birefringence or dichroism induced by the orientation of the azobenzene moieties is observed [10,11]. This indicates that molecular motion takes place in the polymer matrix below the glass transition temperature (T_g). Furthermore, cyclic photoisomerization can be used effectively to fabricate a surface relief structure by exposure to an interference pattern, based on a photoinduced mass transport process of the polymer chains [12–14].

In the field of nanoscale optical science and technology, near-field optics is currently being thoroughly investigated for its use in superfine photolithography and high density optical recording [15,16]. We recently reported on the topographical changes observed on an azopolymer that were induced by the optical near field generated around submicron diameter polystyrene (PS) spheres. We succeeded in transcribing a monolayer of 20 nm diameter spheres on the surface of an azopolymer containing a push–pull type azobenzene derivative to form an indented structure [17]. The structure was thermally stable at room temperature but could be erased by heating the polymer film above T_g. Phase images of the indented structure were observed using tapping mode atomic force microscopy and revealed that the viscoelastic properties of an azopolymer

---

* Corresponding author. Tel.: +81 561 63 6169; fax: +81 561 63 6507.
 E-mail address: e0909@mosk.tytlabs.co.jp (O. Watanabe).

surface treated with spheres change along with the topography. We concluded that the formation of the indented structure we observed is also based on a mass transport process.

The analysis of this mass transport mechanism is a fascinating and important subject from the point of view of polymer photo dynamics and for a wide range of nano-scale to micro-scale surface fabrication applications. Numerous studies involving surface relief gratings (SRG) that attempt to elucidate the mass transfer mechanism have been reported, and some models have been proposed using the electric field gradient, [18] internal pressure [19,20], translation diffusion [21] or interaction between the polar molecules [22]. These models are still evolving as new experimental results are added to existing information concerning this mass transport process. Systematic studies of SRGs in the azopolymers are being continued by several research groups [23,24]. The effect of T_g is an especially interesting issue for analyzing the molecular dynamics, and some fascinating approaches to the examination of the effect have been reported [24]. However, the photochemical effect has not exactly been eliminated as a possible concurrent mechanism for the observed deformation behavior. In order to discuss the effects of the molecular dynamics, the initial isomerization conditions, the quantum yield and the absorption coefficients should be standardized on azopolymers with different values of T_g.

We synthesized several urethane copolymers containing the same amount of push–pull type azobenzene moiety in order to compare their photo-driven mass transport dynamics. The copolymers were synthesized from several kinds of diol and diisocyanate monomers, and they showed different values of T_g, which is controlled by the flexibility of the main chain. In this article, we compare the dependence on T_g of the deformation efficiency during the formation of the SRGs and the indented structures induced by the optical near field. We found that the dependence on T_g changed depending on the irradiation power, and we imagined that this behavior might be related not only to the molecular motion under the irradiation but also to the relaxation after the irradiation was turned off.

2. Experimental

2.1. Samples

A synthetic route for producing the type of azobenzene-containing urethane copolymer used in this report is shown in Fig. 1.

4-N,N-Bis(2-hydroxyethyl)-amino-2,2′-dimethyl-4′-nitro-azobenzene was adopted as an azo-dye moiety diol monomer, and this azo-dye diol was polymerized using other diols and diisocyanate in N-methyl-2-pyrrolidone (NMP) in a nitrogen atmosphere. The ratios of the azobenzene-containing urethane polymers were adjusted such that they contained 45 wt% of the azo-dye moiety.

Thin films of the synthesized polymers were spin-coated onto glass substrates from polymer pyridine solutions after filtration with a Teflon membrane filter (Millipore, 0.22 μm). The films obtained were placed in a vacuum oven at 150 °C for
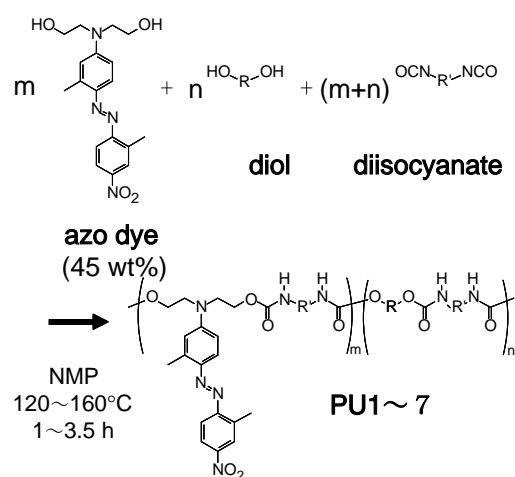

Fig. 1. Synthetic route for azobenzene-containing urethane copolymers.

2 h. The thickness of the films was then measured using a surface profiler (a subsidiary of Veeco Instruments Inc. Dektak3 ST).

2.2. Materials

2.2.1. 4-N,N-Bis(2-hydroxyethyl)-amino-2,2′-dimethyl-4′-nitroazobenzene

Sodium nitrite (15.2 g) dissolved in water (100 mL) was added to a solution of 2-methyl-4-nitroaniline (30.43 g) dissolved in a mixture of water (300 mL) and 36% aqueous hydrogen chloride (180 mL). The solution was maintained at 3 °C for 2 h. m-Tolyldiethanolamine (39.1 g) dissolved in a mixture of water (300 mL) and 36% aqueous hydrogen chloride (30 mL) was added to the resulting solution over a period of 30 min, and the solution was stirred for 4 h at 3 °C. Potassium hydroxide (141.6 g) dissolved in water (800 mL) was added to the reaction mixture to obtain a precipitate. The precipitate was recrystallized from hot ethanol (1.2 L). The recrystallized powder was dissolved in pyridine (500 mL) and was then filtered to remove insoluble material, after which chloroform (1.5 L) was added to the filtrated solution. A crystalline powder was separated out by evaporation of the solvent and the crystals obtained were dried in vacuo to yield the chromophore: 40.2 g; mp 169 °C. ^{1}H NMR (DMSO-d_6) δ 2.6 (s, 3H, CH$_3$), 2.7 (s, 3H, CH$_3$), 3.6 (s, 8H, CH$_2$), 4.8 (s, 2H, OH), 6.6–6.8 (br, 2H, aromatic),7.5–7.8 (m, 2H, aromatic), 8.0–8.3 (m, 2H, aromatic); IR (KBr) 1340 (NO$_2$), 1510 (aromatic C, NO$_2$), 1600 (aromatic C), 2850–3000 (CH$_2$, CH$_3$), 3300 (OH) cm^{-1}.

2.2.2. PU1

A solution of the azo-dye diol (4.53 g) and 2,2-bis (4-hydroxycyclohexyl)propane (1.16 g) in NMP was heated at 60 °C and 4,4′-diphenylmethanediisocyanate (MDI, 4.37 g) dissolved in NMP was added to the solution. The reaction was performed for 30 min at 120 °C and continued for another 60 min at 140 °C. The reaction mixture was diluted with pyridine (150 mL) and was cooled to room temperature. The

solution was added to methanol (4 L) to precipitate the polymer. The polymer that was obtained was purified twice by pyridine–methanol precipitation. The final product was obtained after drying in vacuo, with a yield of 9.3 g.

2.2.3. PU2-7

The polymerization procedure used for the other azobenzene-containing urethane copolymer, PU2-7 was carried out in a same way. The chemical structures of the diol and the diisocyanate that were used as monomers are summarized in Table 1.

2.2.4. PU1

^{1}H NMR (DMSO-d_6) δ 0.71 (cHex-C(CH3)2-cHex), 1.1–2.1 (cHex), 2.60 (CH$_3$), 2.66 (CH$_3$), 3.80 (N–CH$_2$–, aromatic-CH$_2$-aromatic), 4.30 (O–CH$_2$–), 6.82 (aromatic in azobenzene), 7.06 (aromatic derived from diisocyanate), 7.32(aromatic derived from diisocyanate), 7.61 (aromatic in azobenzene), 7.67 (aromatic in azobenzene), 8.07 (aromatic in azobenzene), 8.18 (aromatic in azobenzene), 9.28 (NH), 9.40 (NH), IR (film) 1336 (NO$_2$), 1517 (NO$_2$, aromatic C=C), 1597 (aromatic C=C), 1713 (urethane) cm^{-1}.

2.2.5. PU2

^{1}H NMR (DMSO-d_6) δ 2.60 (CH$_3$ on azobenzene), 2.65 (CH$_3$ on azobenzene), 3.63 (PhN–CH$_2$), 3.77 (azo-N–CH$_2$–, aromatic-CH$_2$-aromatic), 4.21 (PhN–C–CH$_2$–O–), 4.29 (azo-N–C–CH$_2$–O–), 6.60 (aromatic derived from aniline), 6.82 (aromatic in azobenzene and derived from aniline), 7.06 (aromatic derived from diisocyanate), 7.14 (aromatic derived from aniline), 7.32 (aromatic derived from diisocyanate), 7.60 (aromatic in azobenzene), 7.68 (aromatic in azobenzene), 8.07 (aromatic in azobenzene), 8.18 (aromatic in azobenzene), 9.37 (NH), 9.40 (NH), IR (film) 1336 (NO$_2$), 1517 (NO$_2$, aromatic C=C), 1597 (aromatic C=C), 1711 (urethane) cm^{-1}.

2.2.6. PU3

^{1}H NMR (DMSO-d_6) δ 2.08 (CH$_3$ derived from diisocyanate), 2.61 (CH$_3$ on azobenzene), 3.63 (PhN–CH$_2$), 3.78

(azo-N–CH$_2$–), 4.20 (PhN–C–CH$_2$–O–), 4.29 (azo-N–C–CH$_2$–O–), 6.59 (aromatic derived from aniline), 6.81 (aromatic in azobenzene and derived from aniline), 7.03 (NH), 7.14 (NH and aromatic derived from aniline), 7.49 (aromatic derived from diisocyanate), 7.51 (aromatic derived from diisocyanate), 7.58 (aromatic in azobenzene), 7.66 (aromatic in azobenzene), 8.04 (aromatic in azobenzene), 8.15 (aromatic in azobenzene), 8.66 (aromatic derived from diisocyanate), 8.69 (aromatic derived from diisocyanate), 9.40 (aromatic derived from diisocyanate), 9.43 (aromatic derived from diisocyanate), IR (film) 1336 (NO$_2$), 1505 (NO$_2$, aromatic C=C), 1598 (aromatic C=C), 1713 (urethane) cm^{-1}.
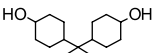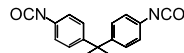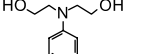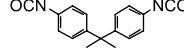
2.2.7. PU4
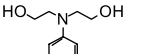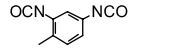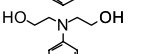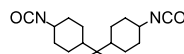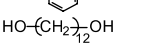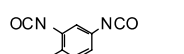
^{1}H NMR (DMSO-d_6) δ 0.4–1.9 (cHex), 2.63 (CH$_3$ on azobenzene), 2.67 (CH3 on azobenzene), 3.53 (PhN–CH$_2$), 3.69 (azo-N–CH$_2$–), 4.06 (PhN–C–CH$_2$–O–), 4.15 (azo-N–C–CH$_2$–O–), 6.59 (aromatic derived from aniline), 6.78 (aromatic in azobenzene and derived from aniline), 7.13 (aroma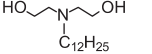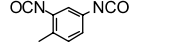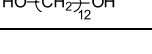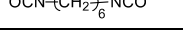tic derived from aniline), 7.61 (aromatic in azobenzene), 7.67 (aromatic in azobenzene), 8.07 (aromatic in azobenzene), 8.18 (aromatic in azobenzene), IR (film) 1336 (NO$_2$), 1504 (NO$_2$, aromatic C=C), 1599 (aromatic C=C), 1706 (urethane) cm^{-1}.

2.2.8. PU5

^{1}H NMR (DMSO-d_6) δ 1.23 (aliphatic), 1.57 (–CO–O–C–CH$_2$–), 2.08 (CH$_3$ derived from diisocyanate), 2.10 (CH$_3$ derived from diisocyanate), 2.62 (CH$_3$ on azobenzene), 3.78 (N–CH$_2$–), 4.02(–CO–O–CH$_2$–), 4.29 (O–CH$_2$–C–N–), 6.82 (aromatic in azobenzene), 7.03 (NH), 7.14 (NH), 7.49 (aromatic derived from diisocyanate), 7.52 (aromatic derived from diisocyanate), 7.60 (aromatic in azobenzene), 7.68 (aromatic in azobenzene), 8.06 (aromatic in azobenzene), 8.17 (aromatic in azobenzene), 8.54 (aromatic derived from diisocyanate), 8.69 (aromatic derived from diisocyanate), 9.30 (aromatic derived from diisocyanate), 9.43 (aromatic derived from diisocyanate), IR (film) 1336 (NO$_2$), 1519 (NO$_2$, aromatic C=C), 1598 (aromatic C=C), 1713 (urethane) cm^{-1}.

Table 1
Monomer composition, glass transition temperature , molecular weight and molar ratio (m and n are shown in Fig. 1) of the azobenzene-containing urethane copolymer used in this work

	Diol	Diisocyanate	T_g (°C)	M_w	M_n	m/n
PU1	HO–⟨cHex⟩–C(CH3)2–⟨cHex⟩–OH	OCN–Ph–C(CH3)2–Ph–NCO	143	18,000	10,000	2.56
PU2	HO–N(Ph)–OH	OCN–Ph–C(CH3)2–Ph–NCO	126	26,000	13,000	2.23
PU3	HO–N(Ph)–OH	OCN–⟨tolyl⟩–NCO	118	23,000	12,000	1.35
PU4	HO–N(Ph)–OH	OCN–⟨cHex⟩–C–⟨cHex⟩–NCO	114	13,000	8500	2.53
PU5	HO–(CH$_2$)$_{12}$–OH	OCN–⟨tolyl⟩–NCO	99	28,000	14,000	1.43
PU6	HO–N(C$_{12}$H$_{25}$)–OH	OCN–⟨tolyl⟩–NCO	72	20,000	9000	1.69
PU7	HO–(CH$_2$)$_{12}$–OH	OCN–(CH$_2$)$_6$–NCO	46	46,000	15,000	1.37

2.2.9. PU6

^{1}H NMR (DMSO-d_6) δ 0.81 (–CH$_3$), 1.1–1.43 (aliphatic), 2.08 (CH$_3$ derived from diisocyanate), 2.61 (CH$_3$ on azobenzene), 2.74 (ali-N–CH$_2$–), 3.78 (azo-N–CH$_2$–), 4.08 (CO–O–CH$_2$–C–N (ali)-), 4.28 (azo-N–C–CH$_2$–O), 6.81 (aromatic in azobenzene), 7.01 (NH), 7.14 (NH), 7.49 (aromatic derived from diisocyanate), 7.51 (aromatic derived from diisocyanate), 7.58 (aromatic in azobenzene), 7.67 (aromatic in azobenzene), 8.04 (aromatic in azobenzene), 8.15 (aromatic in azobenzene), 8.55 (aromatic derived from diisocyanate), 8.68 (aromatic derived from diisocyanate), 9.31 (aromatic derived from diisocyanate), 9.42 (aromatic derived from diisocyanate) IR (film) 1336 (NO$_2$), 1518 (NO$_2$, aromatic C=C), 1598 (aromatic C=C), 1711 (urethane) cm^{-1}.

2.2.10. PU7

^{1}H NMR (DMSO-d_6) δ 1.1–1.6 (aliphatic), 2.64 (CH$_3$ on azobenzene), 2.68 (CH$_3$ on azobenzene), 2.96 (CO–O–CH$_2$–), 3.69 (N–CH$_2$–), 3.91 (CO–N–CH$_2$–), 4.16 (O–CH$_2$–), 6.0–6.9 (NH and aromatic in azobenzene), 7.62 (aromatic in azobenzene), 7.68 (aromatic in azobenzene), 8.08 (aromatic in azobenzene), 8.16 (aromatic in azobenzene), IR (film) 1336 (NO$_2$), 1516 (NO$_2$, aromatic C=C), 1599 (aromatic C=C), 1684 (urethane) cm^{-1}.

2.3. Characterization

The UV–vis spectra were measured on a Shimadzu UV2100 ultraviolet-visible spectrophotometer in film form. All of the differential scanning calorimetry (DSC) thermograms were obtained using a Perkin–Elmer DSC-7 and a TAC 7/DX thermal controller in a nitrogen atmosphere and a heating and cooling rate of 10 °C/min. The number- and weight-average molecular weights (M_n and M_w) of the polymers were measured by gel permeation chromatography (GPC) using a liquid chromatograph (Shimadzu LC-7A) with a column (Shodex KF-807L×2) on dimethylformamide as an eluent, which was calibrated with standard polystyrene. The general properties of these polymers are summarized in Table 1.

2.4. Surface fabrication and analysis

Photoinduced surface modification of the copolymer films was performed by the following procedure (Fig. 2). An aqueous solution including PS spheres (Moritex Co.) was dropped on the surface of the copolymer films, and then the spheres were arranged by a self-assembly process. After drying the samples at room temperature overnight, they were irradiated with a linearly polarized Kr–Ar laser at 488 nm (Omnichrome, 643-AP). Irradiation of the surface of the polymer films was done at normal incidence. The sample films were washed with water and benzene in order to remove the spheres from the surfaces, and were subsequently dried in vacuo at room temperature for 2 days.

A two-beam interferometer was set-up as shown in Fig. 3 and was used for the formation of SRGs on the spin-coated copolymer films. A linearly polarized Ar laser beam at 488 nm (Lexel model 95 ion laser) was split into two by passing the light through a non-polarizing beam splitter. By adjusting
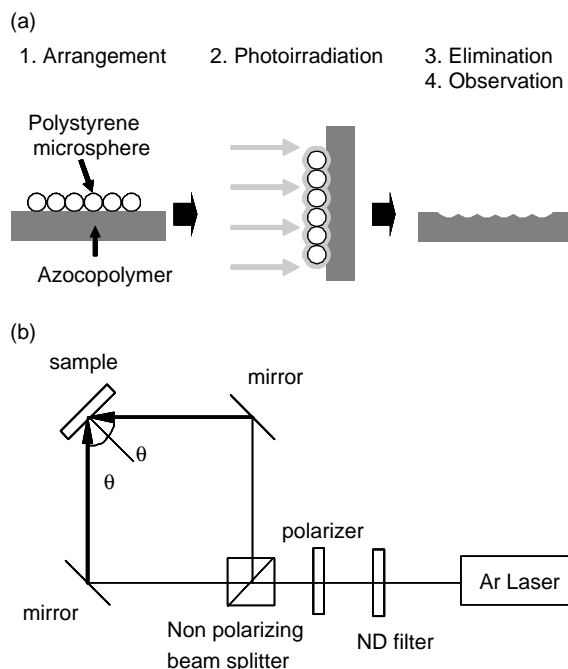

Fig. 2. (a) Schematic representation of a nanopatterning process utilizing polystyrene microspheres as a near-field source. (b) Experimental setup for the SRG fabrication.

a mirror such that the angle of incidence was 45°, an interference beam with a periodicity of $\lambda = 345$ nm was used to expose the copolymer films.

The power density of the irradiation light was determined by measuring the power passing through a pinhole with a diameter of 15 μm. The maximum peak power density was 5.6 W/cm^2. In this case, the average power density was 190 mW/cm^2, which was calculated from the total power (13.5 mW) and the beam area ($\phi = 3$ mm). In this work, we used the maximum peak power density.

The surface structures of the copolymer films were investigated under ambient conditions by contact mode AFM (Digital Instruments Inc., Nanoscope E). For all measurements, a 20-μm scan in contact mode with a microlever force constant of 0.38 N/m was used.

3. Results and discussion

The thickness of the copolymer films was controlled to about 0.5 μm by adjusting the concentration of the solution and the rotational frequency. We reported that the modification depth decreased with decreasing thickness of the sample film, and the depth became saturated after the appropriate irradiation [17]. Films that are sufficiently thick (more than 0.5 μm) are able to exclude the effect of the glass substrate on the mass transfer dynamics. The content of the azobenzene moiety in the azopolymer affects the deformation efficiency on the SRG inscription rate at below 40 wt%. [24] Therefore, we designed the content of the azobenzene moiety to be 45 wt%. In our series, no significant differences in both λ_{max} (approximately 480 nm) and the absorption coefficient (94,300 cm^{-1}) were observed because all the samples have the same azo-dye

concentration and film thickness. The weight-averaged molecular weight also affects the deformation efficiency, [19] so the weight-averaged molecular weights of the copolymers were adjusted in the same way. Under these experimental conditions, only the dependency on T_g of the deformation dynamics can be extracted from the complicated photo-induced-deformation process.

The indented profiles that were transcribed from the arrayed PS microspheres by light irradiation were investigated by AFM. Fig. 3 shows typical AFM images of the surfaces of the fabricated films. The power density was 5.6 W/cm^2 and the irradiation time was 5 min. The surfaces of the films prior to irradiation with the laser beam showed no regular structure. Hexagonal structures with a series of diameters, 250, 500 and 2000 nm, were transcribed directly onto the polymer surfaces,. The indentation structures were formed on the polymer films regardless of T_g. However, the indented forms on the surface of PU7 were slightly distorted in comparison with those on PU1-6. No anisotropic form depending on the polarization direction of the irradiation light was observed on the surface of PU7 despite using PS spheres with a large diameter (2000 nm), even though the anisotropic form appeared in PU-6. In the case of other copolymer films, the anisotropic structures were fabricated by using spheres with a large diameter. The results concerning the surface of PU7 suggest that thermal effects caused by the irradiation cannot be ignored.

Fig. 4 shows the changes in depth and diameter of the indents as a function of T_g. The results obtained from the 250, 500 and 2000-nm microspheres are compared. The indent depth depends on the microsphere diameter, which is caused by the different optical intensity around the microspheres. The depth of the indents increased by tens of or a hundred percent with increasing T_g. On the other hand, the diameter of the indents showed no significant changes dependent on the value of T_g. Only the diameters of the microspheres had any effect in determining the diameter of the indented structures. This phenomenon, which we reported previously when describing the deformation process as a function of irradiation time, [17] is dominated by the optical near field around the polystyrene microspheres. Therefore, any changes in depth would essentially represent differences in molecular mobility between the azo-containing copolymers. Increases in depth with increasing T_g is considered to indicate the opposite tendency, because low T_g polymers are generally more flexible than high T_g polymers. A possible reason for this might be some interaction between the surface of the azopolymer and the polystyrene microspheres. Significant deceases in the formation of the relief gratings by restriction of the surface of the azopolymer induced by ultra-thin top layers of transparent polyelectrolyte have been reported [25]. In order to examine the effect of the microspheres, the formation of SRGs was performed using azopolymers with different T_g values, following the same strategy that was used for near field fabrication.

The structure of the surface relief on the free surfaces induced by two beam interference patterns showed similar tendencies. The relief depth was analyzed by AFM. Fig. 5
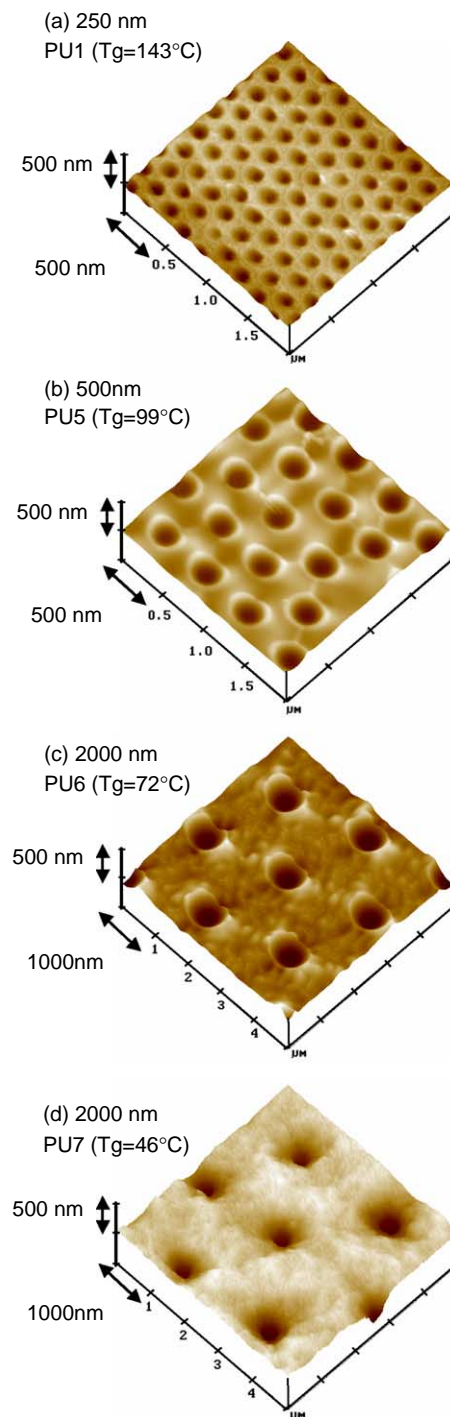

Fig. 3. AFM images of nano-patterned structures formed on various urethane copolymers containing an azobenzene moiety using (a) 250-nm microspheres, (b) 500-nm microsphers, (c) 2000-nm microspheres and (d) 2000-nm microspheres.

shows the changes in the relief depth as a function of T_g. The relief depth also increased with increasing T_g as in the experiment with the microspheres. Therefore, this indicates that there were no effects due to interactions originating from the microspheres. The increasing depth therefore is most likely due directly to the effect of T_g on the photoinduced deformation process. The AFM analyses also revealed that the relief
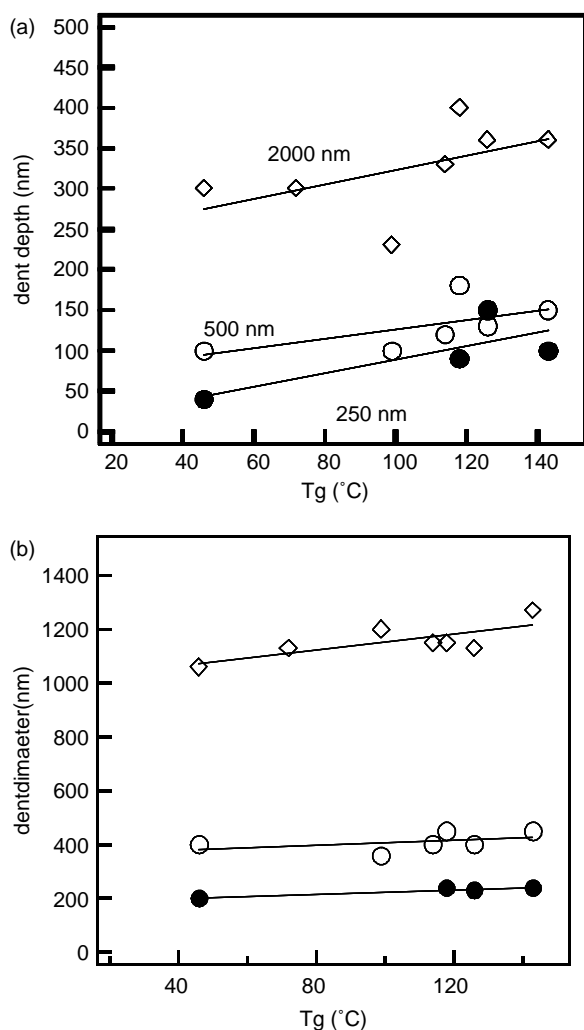
Fig. 4. Changes in (a) the dent depth and (b) the dent diameter as a function of T_g. The solid circles, the open circles and the open rhomboids show the results obtained from the 250, 500 and 2000-nm microspheres, respectively.

structure of PU-7 was distorted when compared with the relief structure of PU1-6 (Fig. 6) As well as the experiment using microspheres, thermal effects should therefore be taken into account to fully analyze the deformation process.
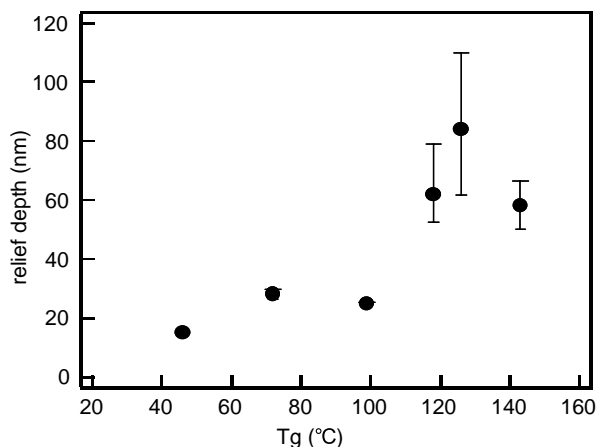

Fig. 5. Changes in the relief depth as a function of T_g. The photo-irradiation was carried out at 5 W/cm². The irradiation time was 5 min.
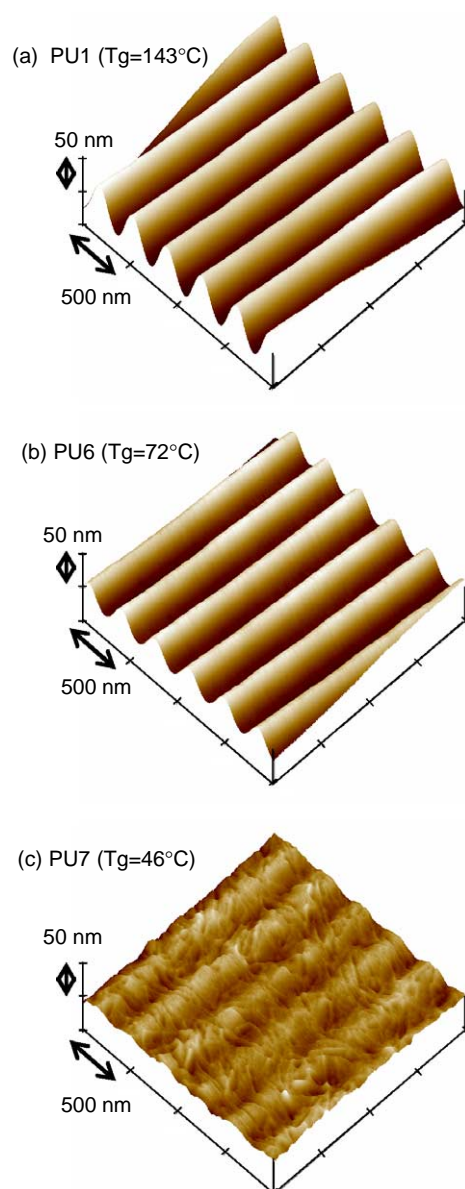
Fig. 6. AFM images of SRGs formed on various urethane copolymers containing an azobenzene moiety using (a) PU1, (b) PU6 and (c) PU7.

The irradiation power discussed above was relatively high. Next, the effects of irradiation power on the T_g dependency of SRG formation were examined. The depths of the relief patterns, as determined by AFM measurement, were compared in the 0.074–5.6 W/cm² range for PU-3 and PU-6. As shown in Fig. 7, the relief depth changes drastically depending on the irradiation power. The relief depth increases sharply above about 0.5–1 W/cm², but no deep relief structures were obtained below that. In cases where there was large deformation, that is, under high power irradiation, the higher T_g azopolymer, PU-3, still showed deeper relief structures than the lower T_g azopolymer, PU-6. Under sufficient irradiation power, it was again shown that the deformation depth increased with increasing T_g. Interestingly, a reverse phenomenon was observed under low power irradiation, when the relief depth obtained from PU-6 was deeper than that from PU-3.
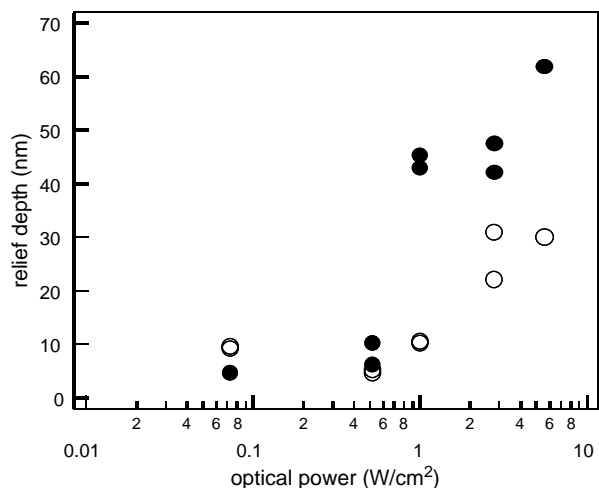
Fig. 7. Changes in the relief depth as a function of irradiation power. The open circles and the solid circles show the results from PU-6 and PU-3, respectively. The irradiation time was 5 min.

To certify this interesting tendency, SRG formation under low irradiation power was examined using azopolymers with different values of T_g. As shown in Fig. 8, the relief depth increased with decreasing T_g of the azopolymer. Although the depth changes were not so large, the depth dependence on T_g was obvious from the experimental results. In the case of indented structures photoinduced by the near-field around microspheres, a similar tendency was also observed.

The relationship between the deformation efficiency and T_g and the inversion of this relationship depending on irradiation power were demonstrated. The first of these relationships shows increasing deformation with increasing T_g of the azopolymer under high power irradiation, while the other shows an increase with decreasing T_g of the azopolymer under low power irradiation. The change in the dependency of the deformation efficiency on T_g due to the change in the
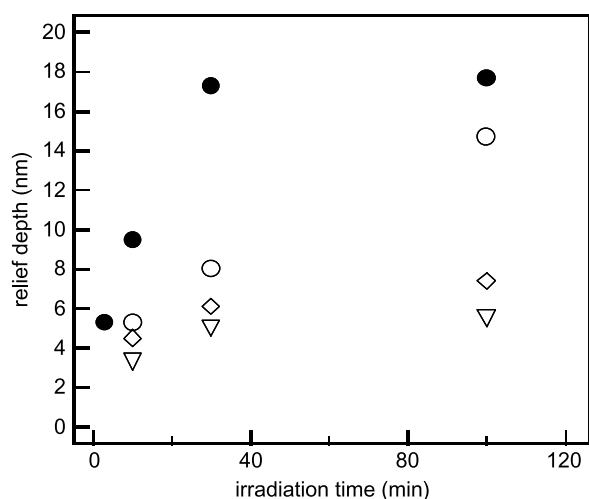

Fig. 8. Changes in the relief depth as a function of time. The photo-irradiation was carried out at 0.074 W/cm². The solid circles, the open circles, the open rhomboids and the open triangles show the results obtained from PU6, PU5, PU4, and PU1, respectively.

irradiation power indicates that, in order to fully analyze the deformation mechanism, it is necessary to consider that the molecular mobility might not only be controlled by T_g, but also that some new factor is affected by light irradiation. There are at least two kinds of physical factor that should be taken into account in the explanation.

One important model for explaining the mass transport at room temperature is photoinduced plasticization on the surface of the amorphous azopolymer through trans–cis–trans isomerization cycles, which occur due to the unstable cis-state [26]. The dependence of the degree of plasticization on the irradiation power could be one of the simple factors giving rise to the inverted relationship. On the other hand, since a deformed structure is generally unstable compared with a flat surface from the point of view of the surface free energy, it should be restored to its former state during the plasticization stage when the force for deformation is removed by cessation of the irradiation. Erasure of the SRG by irradiation with a single laser beam has already been reported [27]. A deformed surface can recover to a flat surface when the positive driving force is removed. Such a recovery process could be another factor influencing the inverted dependency. In addition, thermal effects should be taken into account when considering deformation under high power irradiation. The thermal phenomenon affects the recovery time of the plasticized phenomenon. The disordered surface structure featured in both of the formations we have considered in the case of PU7 (the indented structure and the SRG) would show these thermal effects. Furthermore, we should consider differences in the intermolecular interaction and the elasticity. It has been reported that photo-deformation induced by the plasticization process is affected by every intermolecular interaction of the azobenzene or non-photoactive groups [23]. Since, the bonding pattern of the chromospheres in the urethane copolymer is different from that in a typical acrylate copolymer, we should also look at the mobility of the chromophore in detail. More detailed experimental and theoretical investigation is needed to understand the inversion of the T_g-dependent deformation efficiency.

4. Conclusion

In order to properly examine the effects of molecular mobility on photo-induced deformation, we synthesized novel azobenzene-containing urethane copolymers with different values of T_g. In order to exclude the photoisomerization process, copolymers containing azobenzene moieties with the same structure and content were used. Indented nanostructures induced by the optical near field around polystyrene microspheres and surface relief gratings (SRG) induced by two-beam interference exposure were examined using films of the copolymers. For both fabrication processes, we found the dependence of the deformation efficiency on T_g inverted depending on the irradiation power. This phenomenon allows us to introduce other factors concerning the irradiation power, besides simply the molecular mobility. The degree of plasticization depending on the irradiation power, the recovery

from deformation after the light is turned off, or the thermal effects under high power irradiation might affect the dependence of the relationship on the irradiation power. Although at this stage, it is difficult to explain the exact mechanism causing the surface deformation, this discovery could be a clue to the mechanism of photo-induced surface deformation.

References

[1] Gibbons WM, Shannon PJ, Sun ShT, Swetlin BJ. Nature 1991;351:49.
[2] Kumar GS, Neckers DC. Chem Rev 1989;89:1915.
[3] Burland DM, Miller RD, Walsh CA. Chem Rev 1994;94:31.
[4] Moener WE, Silence SM. Chem Rev 1994;94:127.
[5] Ichimura K. Chem Rev 2000;100:1847.
[6] Delaire JA, Nakatani K. Chem Rev 2000;100:1817.
[7] Natansohn A. Azobenzene-containing materials. Weinheim: Wiley–VCH Verlag Gmbh; 1999.
[8] Viswanathan NK, Kim DY, Bian S, Williams J, Lie W, Li L, et al. Mater Chem 1999;9:1941.
[9] Natansohn A, Rochon P. Chem Rev 2002;102:4139.
[10] Todorov T, Tomova N, Nikolova L. Opt Commun 1983;47:123.
[11] Todorov T, Nikolova L, Tomova N. App Opt 1984;23:4309.
[12] Rochon P, Batalla E, Natansohn A. Appl Phys Lett 1995;66:136.
[13] Kim DY, Li L, Kumar J, Tripathy SK. Appl Phys Lett 1995;66:1166.
[14] Ramanujam PS, Holme NCR, Hvilsted S. Appl Phys Lett 1996;68:1329.
[15] Betzig E, Trautman JK, Wolfe R, Gryorgy EM, Finn PL, Kryder MH, et al. Appl Phys Lett 1992;61:142.
[16] Ohtsu M, Hori H. Near-field nano-optics. New York: Kluwer Academic; 1999.
[17] (a) Kawata Y, Egami C, Nakamura O, Sugihara O, Okamoto M, Tsuchimori M, et al. Opt Commun 1999;161:6.
　　(b) Watanabe O, Ikawa T, Hasegawa M, Tsuchimori M, Kawata Y, Egami C, et al. Mol Cryst Liq Cryst 2000;345:305.
　　(c) Ikawa T, Mitsuoka T, Hasegawa M, Tsuchimori M, Kawata Y, Egami C, et al. J Phys Chem B 2000;104:9055.
　　(d) Hasegawa M, Ikawa T, Tsuchimori M, Watanabe O, Kawata Y. Macromolecules 2001;34:7471.
　　(e) Watanabe O, Ikawa T, Hasegawa M, Tsuchimori M, Kawata Y. Appl Phys Lett 2001;79:1366.
　　(f) Ikawa T, Mitsuoka T, Hasegawa M, Tsuchimori M, Watanabe O, Kawata Y. Phys Rev B 2001;64:195408.
　　(g) Hasegawa M, Keum CD, Watanabe O. Adv Mater 2002;14:1738.
　　(h) Keum CD, Ikawa T, Tsuchimori M, Watanabe O. Macromolecules 2002;36:4916.
[18] Kumar J, Li L, Jiang XL, Kim DY, Lee TS. Appl Phys Lett 1998; 75:1878.
[19] Barrett CJ, Natansohn A, Rochon P. J Phys Chem 1996;100:8836.
[20] Sumaru K, Yamanaka T, Fukuda T, Matsuda H. Appl Phys Lett 1999;102: 16074.
[21] Lefin O, Fiorini C, Nunzi JM. Pure Appl Opt 1998;7:71.
[22] Pedersen TG, Jephansen PM. Phys Rev Lett 1997;79:2470.
[23] Börger V, Kuliskovska O, Kati G-H, Stumpe J, Huber M, Menzel H. Macromol Chem Phys 2005;206:1488.
[24] Fukuda T, Matsuda H, Shiraga T, Kimura T, Kato M, Viswanathan NK, et al. Mactromolecules 2000;33:4220.
[25] Viswanathan NK, Balasubramanian S, Li L, Kumar J, Tripathy SK. J Phys Chem B 1998;102:6064.
[26] Ho MS, Natansohn A, Barrett C, Rochon P. Can J Chem 1995;73:1773.
[27] Jiang XL, Li L, Kumar J, Kim DY, Tripathy SK. Appl Phys Lett 1998;72: 2502.